Nanoscale

PAPER

View Article Online
View Journal | View Issue

Cite this: *Nanoscale*, 2026, **18**, 7002

The bis-salphen Zn(II) unit: a versatile building block for self-assembled heteroleptic coordination cages

Leonardo Donaggio,[a] Kristian Schweimer,[b] Frank W. Heinemann,[c] Janosch Hennig[b,d] and Hannah Kurz *[a]

Heteroleptic coordination cages enable not only a high control over the cavity properties but also multifunctionality. However, their synthesis is far from trivial and often relies on precious 4d and 5d transition metals such as Pd(II). The transfer to more cost-effective, earth abundant metal ions such as Zn(II) is highly desirable for increasing their application potential in real-life scenarios. In this work, we report on a self-assembly strategy employing the ditopic Zn(II) bis-salphen unit **Zn_2L** in combination with tritopic pyridyl-based ligands to construct novel prismatic cages. As a proof of concept, two distinct cages are presented, utilizing either a phenyl- or triazine-based tritopic ligand (cage **1** and cage **2**, respectively). Both cages exhibit remarkable stability at low concentrations while displaying dynamic behaviour at high concentrations. Investigation of their photophysical properties reveals a striking "on–off" emission behaviour: the phenyl-based cage **1** features a significant orange emission (Φ = 6%), while cage **2** is non-emissive. This emission quenching can be attributed to the electron-withdrawing nature of the triazine ligand, which dominates the electronic relaxation pathway of the **Zn_2L** unit. Although both cages successfully bind aromatic guests in host–guest studies, their encapsulation results in partial cage decomposition, which prevents further investigation of whether cage **1** qualifies as an optical sensor material. However, the findings herein introduce a versatile route to emissive bis-salphen coordination cages, marking a significant step towards developing new heteroleptic zinc(II) cages for optical sensing.

Received 29th October 2025,
Accepted 19th February 2026

DOI: 10.1039/d5nr04564a

rsc.li/nanoscale

Introduction

A well-defined, and highly tuneable cavity can give rise to a remarkable host–guest chemistry enabling stabilization of reactive molecules,[1–3] (photo)catalysis,[4–6] separation/purification,[7–9] and sensing.[10–12] One compound class that allows the targeted tuning of cavity properties including size and shape are coordination cages. These molecular nanocapsules stand out due to their facile synthesis based on (subcomponent) self-assembly[13,14] and their high solubility in a wide range of solvents including water.[15,16] Most literature-known cages are of homoleptic, highly symmetrical nature. In contrast, heteroleptic cages are composed of at least two different ligands. One key advantage of heteroleptic cages is the possibility to anchor different ligand units with varying properties into the cage scaffold, enabling multifunctionality. However, the controlled synthesis of these heteroleptic structures is a challenging task as these require a high selectivity for the coordination of two different ligands. Therefore, the main synthetic strategies are based on shape-complementary ligands,[17–19] steric control,[20–23] or charge repulsion control.[24–26] Most reported cages are based on square-planar dictating Pd(II) and Pt(II) metal ions.[27–29] Recently, Pd(II) and Pt(II) examples of heteroleptic cages with up to four different ligands have been reported.[30–32] Although these cages offer the advantage of high stability due to the inertness of the coordinative bond, their high cost often prevents the transfer into real-life applications. Consequently, replacing these precious metal ions with cheaper 3d transition metal ions is highly beneficial. A few examples of these heteroleptic 3d transition metal based cages have been reported, which are mostly based on subcomponent self-assembled imine-based zinc(II) or iron(II) cages.[33–36] Furthermore, Zhang *et al.* have recently reported on salphen-based heteroleptic Co(III) cages that are based on the shape-complementary approach.[37]

The readily accessible bis-salphen zinc(II) motif (**Zn_2L**) has been extensively explored for the formation of supramolecular architectures,[38] catalysis,[39] and optoelectronic applications.[40]

[a]*Inorganic Chemistry IV, University of Bayreuth, 95447 Bayreuth, Germany. E-mail: hannah.kurz@uni-bayreuth.de*
[b]*Department of Biochemistry IV – Biophysical Chemistry, University of Bayreuth, 95447 Bayreuth, Germany*
[c]*Friedrich-Alexander-University Erlangen-Nürnberg (FAU), Department of Chemistry and Pharmacy, Inorganic Chemistry, 91058 Erlangen, Germany*
[d]*Molecular Systems Biology Unit, European Molecular Biology Laboratory (EMBL), 69117 Heidelberg, Germany*

Besides the facile modular synthesis based on commercially available compounds, a main advantage is the high tuneability of the $\mathbf{Zn_2L}$ motif. Self-assembly of the binuclear complex with ditopic pyridyl-type ligands resulted in the formation of two-dimensional molecular boxes as described by Kleij *et al.*[38,41] However, box-like structures do not always exhibit satisfactory host–guest chemistry due to the lack of a 3D confinement. It is intuitive to assume that increasing the topicity of the pyridyl moiety containing ligand will result in discrete molecular cages.

In this paper we report on two novel heteroleptic trigonal prismatic cages based on the $\mathbf{Zn_2L}$ bis-salphen motif. We classify these cages as heteroleptic, as the bis-salphen unit functions as an active part of the cage scaffold and defines the cavity of the cages similar to cages recently classified as heteroleptic by Clever.[37] These cages $\mathbf{(Zn_2L)_3A_2}$ and $\mathbf{(Zn_2L)_3B_2}$ are formed in a quantitative manner upon self-assembly of $\mathbf{Zn_2L}$ with the tritopic ligands 1,3,5-tri(4-pyridyl)benzene (**A**) and 2,4,6-tri(4-pyridyl)-1,3,5-triazine (**B**), respectively. The nature of the tritopic ligand strongly affects the photophysical properties of the cages, as $\mathbf{(Zn_2L)_3A_2}$ shows a strong orange emission while $\mathbf{(Zn_2L)_3B_2}$ is non-emissive. To investigate whether $\mathbf{(Zn_2L)_3A_2}$ qualifies as an optical sensor towards guest molecules, the host–guest properties of these cages were determined.

Results and discussion

Synthesis and characterization

Bis-Zn-salphen ($\mathbf{Zn_2L}$) complex was synthesized using a modified literature procedure[38] as described in chapter 2.1 of the SI. $\mathbf{Zn_2L}$ was characterized by nuclear magnetic resonance (NMR) spectroscopy, elemental analysis, and electrospray ionization time-of-flight (ESI-TOF) mass spectrometry (MS) (details are given in chapter 2.1 in the SI). Coherently with the coordinative preferences of the d^{10} Zn(II) ion, the square-planar coordination sphere dictated by the salphen ligand is overcome by axial coordination of water molecules leading to an octahedral coordination geometry. The presence of the additional axial water ligands was confirmed by elemental analysis. As Zn(II) complexes in a square-planar dictating chelate ligand tend to aggregate in the absence of potent Lewis bases, *tert*-butyl substituents were introduced to prevent this effect.[38,42]

Trigonal prismatic metal–organic cages **1** ($\mathbf{(Zn_2L)_3A_2}$) and **2** ($\mathbf{(Zn_2L)_3B_2}$) were synthesized upon self-assembly of 3 equivalents of $\mathbf{Zn_2L}$ with 2 equivalents tris-1,3,5-(4-pyridyl)benzene (**A**) and tris-2,4,6-(4-pyridyl)-1,3,5-triazine (**B**) in dichloromethane (DCM), respectively as depicted in Fig. 1. The mild reaction conditions – room temperature for 3 h – point towards a low energy barrier and a high driving force to form the thermodynamically favoured neutral cages. It is crucial to perform the self-assembly in a non-coordinating solvent such as DCM to prevent competing coordination by solvent molecules. While $\mathbf{Zn_2L}$ itself is not soluble enough for ^{1}H NMR analysis in chlorinated non-coordinating solvents, quantitative cage formation occurred upon stoichiometric reaction with ligands **A** or **B** in DCM.

NMR characterization. Only one set of sharp signals was obtained in ^{1}H NMR spectra of the individual cages indicating the formation of discrete cage species (Fig. S5 and S18). While the expected shifts of the complex $\mathbf{Zn_2L}$ could not be followed due to its low solubility in DCM, the signals of the tritopic ligands are significantly upfield-shifted hinting towards an altered magnetic environment. This is due to coordination of the pyridyl nitrogens to the Zn(II) metal centres (see Fig. 2a and b for aromatic region, Fig. S6 and S19 for full spectrum). The full 1D and 2D NMR characterization enabled the assignment of all proton and carbon signals (see chapter 2.2. and 2.3. in the SI). Diffusion ordered spectroscopy (DOSY) NMR spectra confirmed the formation of one single discrete species

Hannah Kurz

Hannah Kurz is a Junior Professor of Inorganic Chemistry at the University of Bayreuth, Germany. After receiving her PhD in 2022, she conducted postdoctoral research at the University of Cambridge, UK, focusing on robust zinc(II) coordination cages. Since establishing her independent group in December 2024, her research has centred on the development of sustainable heteroleptic coordination cages. Her team explores the intersection of supramolecular chemistry and photochemistry, specifically targeting innovative solutions for optical sensing and photocatalysis.

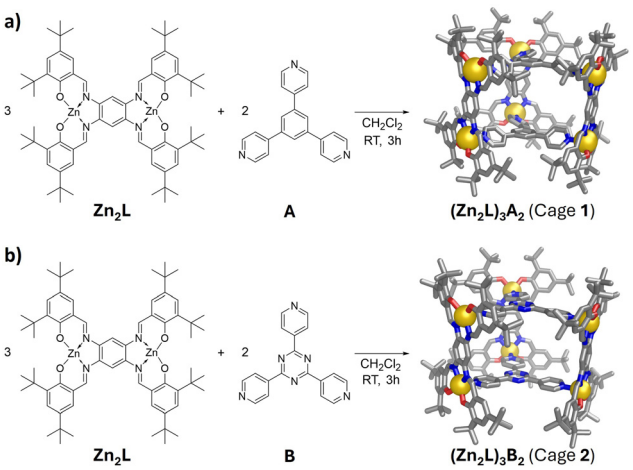

Fig. 1 Self-assembly of $\mathbf{Zn_2L}$ with tritopic ligand **A** or **B**, to form cage **1** (a) and cage **2** (b), respectively. The cages are illustrated as MM2 models. Colour code: C (grey), N (blue), O (red), Zn (yellow). Hydrogens are omitted for clarity.

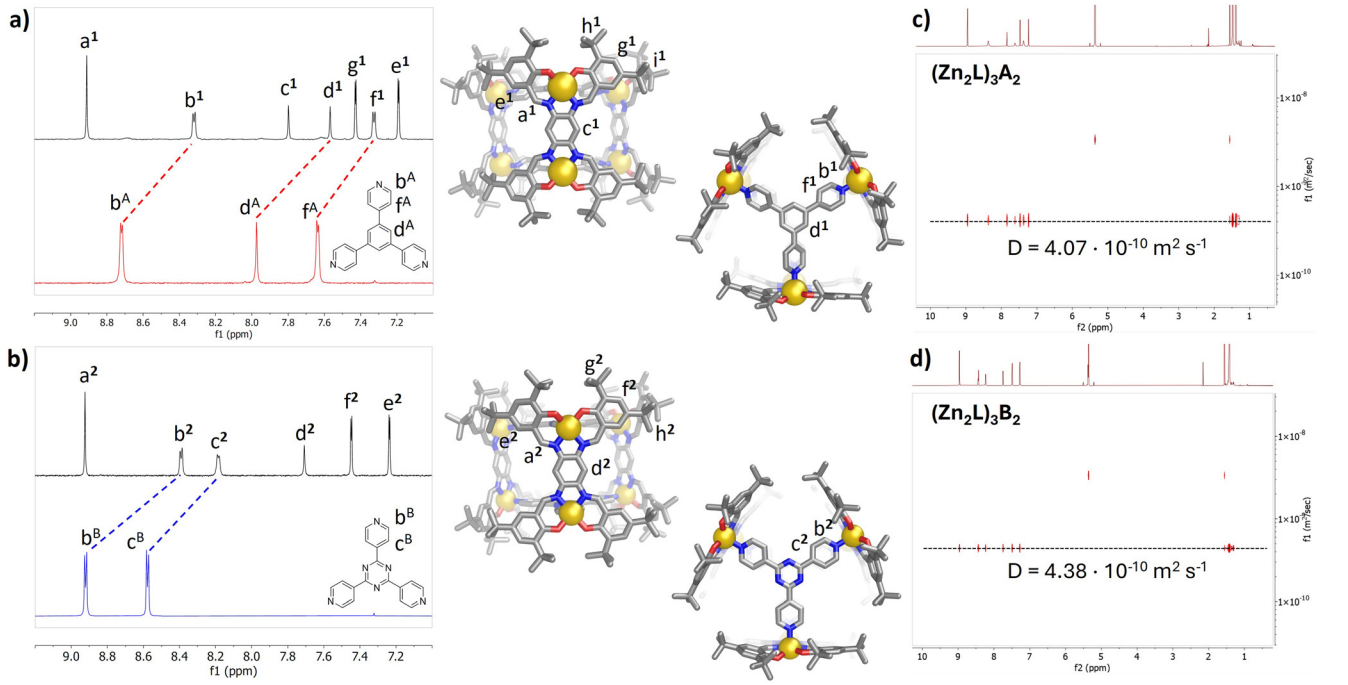

Fig. 2 Stacked ^{1}H NMR spectra of cage **1** with ligand **A** (red, a) and cage **2** with ligand **B** (blue, b) with NMR assignment. DOSY NMR spectra of cage **1** (c) and cage **2** (d).

for each cage with diffusion coefficients of 4.07×10^{-10} m^2 s^{-1} for cage **1**, and 4.38×10^{-10} m^2 s^{-1} for cage **2** (Fig. 2c and d). This translates to a solvodynamic radius of 13.1 Å for cage **1** and 12.2 Å for cage **2**. These values are in accordance with the average radius of 11.7 Å for **1** and 11.4 Å for **2** determined from the MM2 models of the cages (see Fig. S15 and S28 in the SI).

Mass spectrometric characterization. Mass spectrometry (MS) of the neutral cages was performed *via* ESI-TOF mass spectrometry in a DCM : MeOH 1 : 1 solvent mixture. While the addition of the potent Lewis base MeOH is not ideal as it could act as a competing ligand and lead to cage decomposition, the addition of a polar solvent is a requirement for ESI-TOF MS experiments. In control NMR experiments of cage **1** and **2** in a 1 : 1 DCM : MeOH solvent mixture (c = 0.5 mM) only NMR signals of the intact cages were obtained (Fig. S16 and S29). However, precipitation was observed pointing towards a low solubility in this solvent mixture. Under MS conditions, the expected MS signals of the neutral cages at 4008 m/z (cage **1**) and 4014 m/z (cage **2**) could not be observed. Nevertheless, a high number of fragments (*e.g.* for cage **1**: $(Zn_2L)_1A_2$ + Na^+, $(Zn_2L)_2A_1$ + Na^+, and $(Zn_2L)_2A_2$ + Na^+) was observed, strongly hinting towards the presence of the cages (see Fig. S17 and S30 int the SI). The combination of the rather harsh MS conditions, with the presence of the potent Lewis base MeOH in high excess and the low concentration might be the reason for the strong fragmentation.

Structure analysis. To gain further insight into the cage structure, MM2 simulations were performed for both cages (see Fig. S31 and S32 in the SI). From a structural perspective, the two cages feature a similar trigonal prismatic geometry with comparable dimensions. However, there are key differences that distinguish these two species. Steric hindrance between the protons of pyridyl and central phenyl rings of ligand **A**, results in a twisting of the pyridyl rings as illustrated in Fig. S31 in the SI. In contrast, ligand **B**, owing to the reduced steric hindrance of the triazine nitrogen atoms, features increased rotational freedom, thereby facilitating the adoption of a co-planar conformation within the central scaffold of cage **2** (see Fig. S32 in the SI).

Crystals of cages **1** and **2** suitable for single X-ray analysis were obtained *via* low temperature (8 °C) liquid–liquid diffusion of CH_3CN into a DCM solution of cage **1** and **2**, respectively (see chapter 3 in the SI for crystallographic details). Please note, that the low quality of the crystal data is due to a high amount of unresolved solvent molecules, which required the application of a solvent mask. The crystal structures of both cages confirmed the square-pyramidal coordination geometry of the zinc(II) metal centre, in which the zinc (II) metal centre is slightly moved out of the N_2O_2 plane of the bis-salphen ligand. In accordance with the MM2 models, the steric hindrance of the phenylic protons within the tritopic ligand **A** of cage **1** results in an out-of-plane twisting of the phenyl rings as shown in Fig. S33–S35 in the SI. In contrast to the MM2 models of cage **1**, in which the bis-salphen plane is oriented at nearly 90° relative to the plane of the tritopic ligand **A**, the crystal structure revealed a deviation from this orthogonal alignment. This results in the phenyl rings being

offset from each other, which has significant impact on the cavity shape. In contrast, such a distortion was not observed in the crystal structure of cage **2**. In accordance with the MM2 models, the triazine ligand **B** is planar leading to a nearly perfect 90° angle between the salphen chelate ligand and **B** (see Fig. S37–S39 in the SI).

In the crystal structures of **1** and **2**, a high number of solvent molecules is present. Although there are no strong intermolecular interactions such as hydrogen bonds, the molecular packing of the cages is highly ordered. The cages are aligned in such a way that the prismatic cages are forming densely packed planes that are ordered in an ABAB manner (see Fig. S36 for cage **1** and Fig. S40 for cage **2** in the SI).

Investigation of the dynamic nature

As the cages are only held together by coordinative bonds, investigating their stability at different concentrations is crucial for determining their application potential. ^{1}H NMR dilution series confirmed that both cages are stable even at low concentrations of up to 7.5 μM (see chapter 4.1. and 4.2 in the SI for details). In all cases no free signals of the tritopic ligands **A**/**B** appear and no visible precipitate formed due to the formation of free **Zn_2L**. However, a significant broadening of the signals of the tritopic ligands **A**/**B** was observed upon concentration increase, pointing to a highly dynamic ligand exchange (see Fig. 3a and b for the aromatic region; see Fig. S41 and S46 in the SI for aromatic region and Fig. S42 and S47 in the SI for zoom into the aliphatic region). We attribute this concentration-dependent effect to the ability of the tritopic ligands to undergo exchange with neighbouring cages, facilitated by the labile nature of the Zn–N bond. As anticipated, this effect becomes more pronounced at higher concentrations.

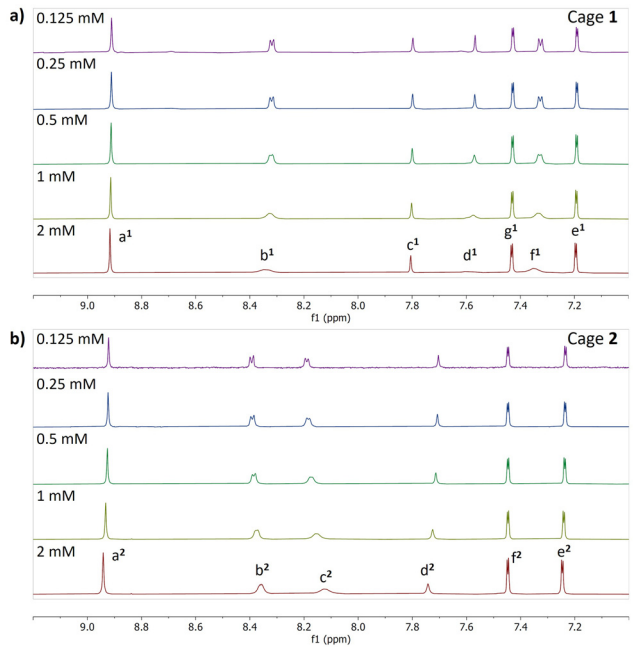

Fig. 3 Variable concentration ^{1}H NMR spectra of cage **1** (a) and cage **2** (b), respectively.

Along with the signal broadening, concentration-dependent chemical shift perturbations were observed for certain proton signals. The protons of the tritopic ligand **A** within cage **1** are downfield shifted upon concentration increase. While these concentration-dependent shifts are small, they are more pronounced upon addition of excess ligand **A** to cage **1** (see Fig. S43 in the SI). In agreement with the more downfield-shifted signals of the free ligand **A** (see Fig. 2), we conclude that these shifts are based on a highly dynamic intermolecular exchange of the tritopic ligand. However, the opposite effect – an upfield-shift – was observed for the protons of the tritopic ligand **B** within cage **2**. Again, these shifts are only small upon concentration increase, but much more pronounced upon addition of excess **B** (see Fig. S48 in the SI). As the signals of the free ligand **B** are also downfield-shifted compared to their signals within cage **2** (see Fig. 2b), there must be a competing shielding effect leading to an overall upfield-shift. While small upfield-shifts are also observed for proton h^2, downfield-shifts were observed for protons a^2, d^2 and g^2 (see Fig. 3b). These chemical shift perturbations are less pronounced but in agreement with host–guest studies of the triazine guest **G2**, which led to similar shifts upon encapsulation (see paragraph Host–Guest Chemistry and Fig. S72 in the SI). These findings hint towards a certain amount of tritopic ligand **B** being encapsulated within cage **2**, particularly if present in excess. In contrast, an excess of **Zn_2L** led in both cases to a sharpening of the signals in the ^{1}H NMR spectra implying a more static situation (see Fig. S43 and S48 in the SI). Please note, that an intermediate exchange was observed, which prevents the monitoring of the exchange through EXSY NMR experiments at 298 K (see Fig. S44 in the SI). Performing the EXSY experiment on a 1 GHz NMR spectrometer at 278 K results in a new set of signals that can be assigned to the free ligand. However, these signals are still rather broad, which again limits a detailed monitoring of the exchange by EXSY studies (see Fig. S45 in the SI).

Photophysical characterization

The relatively high stability of the cages even at low concentrations allows the investigation of their optical properties *via* UV-Vis and photoluminescence spectroscopy. Interestingly, cages **1** and **2** show an "on–off" behaviour concerning their emission: while cage **1** features a strong orange emission, cage **2** is non-emissive (see Fig. 4a and b). While the tritopic ligands **A** and **B** and the ligand **H_2L** in DCM are non-emissive, a significant emission has been observed for the bis-salphen unit **Zn_2L** (see Fig. S49 for **A**, **B**, and **H_2L** and Fig. S50 and Tables S2, 3 for **Zn_2L** in the SI). Due to the low solubility of the complex **Zn_2L** in DCM, the weakly coordinating solvent acetone and the potent Lewis base pyridine were chosen as solvents for these experiments. Both solutions show similar absorption spectra composed of a maximum absorption band around 520 nm. In both cases a vibrational fine structure was obtained, leading to shoulders accompanying the main

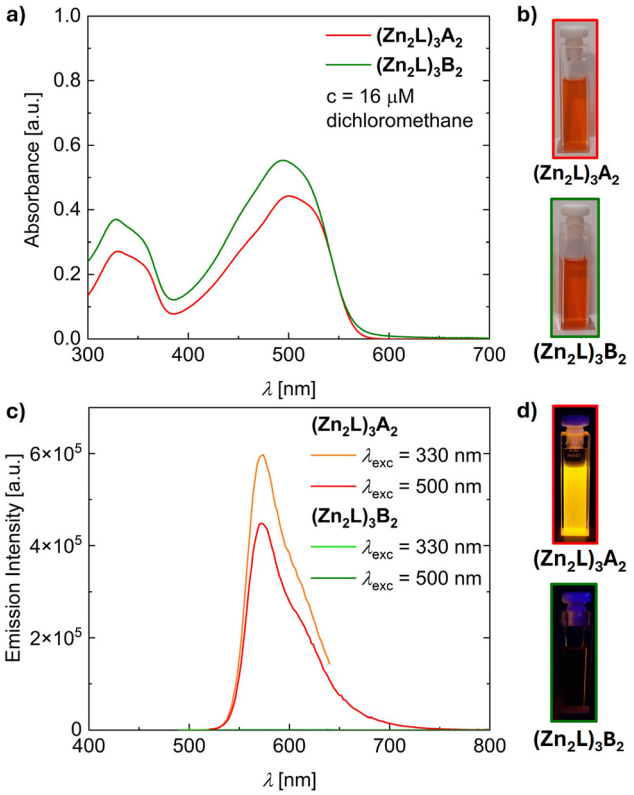

Fig. 4 Absorbance (a) spectra of cage **1** and **2** in DCM (c = 16 μM, 2 mm cuvette) and photos of the cuvettes (b). Emission (c) spectra of cage **1** and **2** in DCM (c = 16 μM, 2 mm cuvette) and photos of the cuvettes (d). Please note that for the photos, 1 cm cuvettes have been used for illustration purposes (λ_{exc} = 365 nm).

absorption band. The axial coordination of pyridine resulted in a 10 nm redshift of the major band and shoulders and a decrease of the extinction coefficient ε from approximately 73 000 M^{-1} cm^{-1} to 66 000 M^{-1} cm^{-1} (see Table S2 in the SI for details). While both solutions are emissive, the emission maximum of the pyridine solution is red shifted ($\lambda_{em,acetone}$ = 557 nm *vs.* $\lambda_{em,pyridine}$ = 566 nm) and features an approximately twofold stronger emission intensity than the acetone solution (see Fig. S50b in the SI). This is further reflected by higher quantum yields of the pyridine solution ($\Phi_{\mathbf{Zn2L},acetone}$ = 4.9% *vs.* $\Phi_{\mathbf{Zn2L},pyridine}$ = 9.8%). Photoluminescence lifetimes were recorded at the respective emission maxima (see Table S3 in the SI). The lifetimes τ reflect the qualitative order of emission intensity, as the $\mathbf{Zn_2L}$ pyridine solution shows a significant longer lifetime (τ = 0.96 ns), which could be best fitted with a monoexponential fit function. In contrast, a biexponential decay function needs to be applied for fitting the acetone solution with the main component being τ_1 = 0.44 ns. The shorter lifetime and the lower emission intensity of the acetone solution might be based on aggregation-caused emission quenching, which was observed for a high number of salphen based zinc(II) complexes.[43–45]

DCM solutions of cage **1** and cage **2** show similar absorption behaviour compared to the $\mathbf{Zn_2L}$ subunit. A minor absorption band around 330 nm and a major absorption band around 500 nm with vibrational fine structure was observed (see Fig. 4a). As each cage molecule is composed of three $\mathbf{Zn_2L}$ units, the extinction coefficient ε is strongly increased compared to the $\mathbf{Zn_2L}$ subunit (cage **1**: λ_{max} = 500 nm, ε_{max} = 138 000 M^{-1} cm^{-1}; cage **2**: λ_{max} = 495 nm, ε_{max} = 173 000 M^{-1} cm^{-1}). While cage **1** shows a strong orange emission at $\lambda_{em,max}$ = 574 nm ($\Phi_{\mathbf{1},DCM}$ = 6.6%), cage **2** is emission silent (see Fig. 4b). The radiative decay of cage **1** could be best fitted by a monoexponential decay function resulting in a lifetime of τ = 1.07 ns (see Table S3 and Fig. S51 in the SI for details). The complete emission quenching for cage **2** cannot be attributed to decomposition effects, as NMR dilution experiments confirmed intact cages even at sub-UV-Vis concentrations. Furthermore, the electronic properties at least of the ground state of cages **1** and **2** must feature a high similarity, given their highly similar absorption spectra. Most likely the emission quenching is based on the electron withdrawing nature of the triazine ligand **B** within cage **2**, leading to a fast non-radiative decay.

Investigation of mixed assemblies

A mixed self-assembly reaction was performed with 3 eq. of $\mathbf{Zn_2L}$ and 1 eq. of **A** and **B** each as depicted in Fig. 5 (see chapter 6 in the SI for details). The self-assembly was performed under similar conditions as previously described for cages **1** and **2**. The ^{1}H NMR spectrum of the mixed assembly shows the presence of eight new signals in the aromatic area. Additionally, five more signals are overlapping with the peaks of the other two cages leading to broadening of the signals (see Fig. S52 for full integrated ^{1}H NMR spectrum and Fig. S53 for zoom into aliphatic region). We infer the novel structure is a mixed cage with stoichiometry $\mathbf{(Zn_2L)_3AB}$, in accordance with the number of new signals. While some proton signals exhibit a stronger chemical shift perturbation in the mixed assembly $\mathbf{(Zn_2L)_3AB}$ (*e.g.* imine protons a^1 and a^2 and the phenylic protons c^1 and d^2), all signals are affected by the change of the tritopic ligand. This finding is in accordance with the crystal structure of cage **1**, which confirms a strong effect of the tritopic unit on the overall cage structure. The formation of the statistical mixture could be furthermore performed in a successive manner (see Fig. S54 and S55 in the SI). The formation of the statistical mixture of the cages is a fast process, as time-dependent changes after an initial interval of 10 min could not be observed (see Fig. S56 in the SI).

To determine whether the mixed cage assembly is emissive, the percentages of respective cages (**1**, **2**, and mixed) were compared to the respective emission intensity. Therefore, a series of self-assemblies with varying **A** : **B** ratios was performed (see Fig. S57 and S58 for ^{1}H NMR spectra). The percentages of the respective cages were determined upon integration of the proton signals at 7.80 ppm (cage **1**), 7.76 ppm (mixed cage), and 7.71 ppm (cage **2**) (see Table S4 in the SI for details).

The absorbance and emission spectra of the assemblies with **A** : **B** ratios of 2 : 1, 1 : 1, and 1 : 2 were recorded and are shown in Fig. S59 in the SI. The emission intensity at the emis-

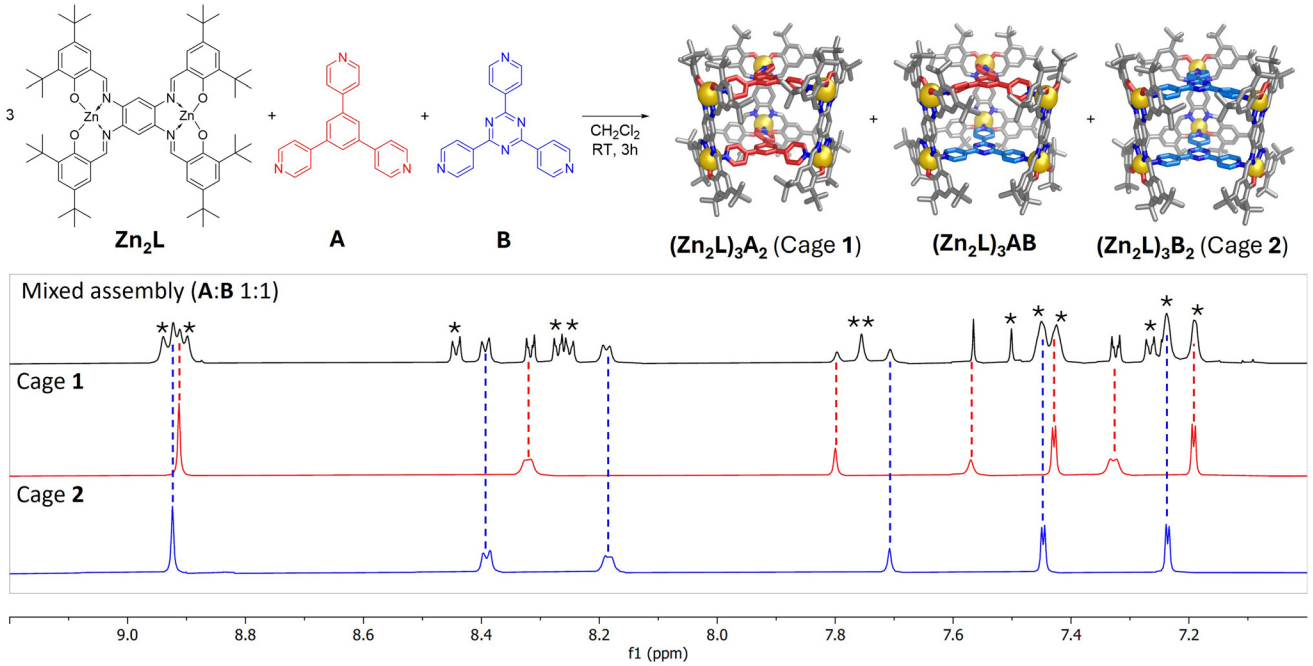

Fig. 5 Self-assembly of statistical mixture of cage **1** ($(Zn_2L)_3A_2$), cage **2** ($(Zn_2L)_3B_2$), and novel $(Zn_2L)_3AB$. For clarity, ligand **A** is coloured red, and ligand **B** is coloured blue. ^{1}H NMR spectra [0.5 mM] of the mixed assembly (top) stacked with cage **1** (middle, red spectra), and cage **2** (bottom, blue spectra). New signals are marked with an asterisk.

sion maximum of $\lambda_{em,max}$ = 574 nm was determined and normalized (see Table S5 in the SI). A comparison of the cage percentages and the emission intensity confirmed that the emission is solely based on cage **1**, while the mixed cage $(Zn_2L)_3AB$ in accordance with cage **2** is non-emissive. This quenching effect even within the mixed $(Zn_2L)_3AB$ cage was furthermore confirmed by the photoluminescence lifetimes, which are τ = 1.07 ns for all assemblies hinting towards the same species – cage **1** – being responsible for the emission in all mixed assemblies (see Fig. S59d and Table S5 in the SI).

Host–guest chemistry

The smaller inner cavity of cage **1** compared to cage **2** might impact the host guest-chemistry of the two trigonal prismatic structures. Molovol[46] calculations based on the MM2 models confirmed that the available cavity space of cage **1** is 27% more compact (933 Å^3) in comparison to cage **2** (1277 Å^3) (see chapter 7 and Fig. S60 and S61 in the SI). Whilst these volumes are significantly larger relative to previously synthesized and published molecular capsules,[47] the geometry of the structures must be considered for its guest binding ability. According to Rebek's 55% rule,[48] and given the trigonal prismatic cavity shape, we explored 1,3,5-triphenylbenzene (**G1**) and 2,4,6-triphenyl-1,3,5-triazine (**G2**) as guest molecules. These display surface volumes (calculated using Molovol[46]) of 542 Å^3, and 521 Å^3, respectively. ^{1}H NMR titration series were conducted to investigate the host–guest chemistry of cage **1** and cage **2** (see chapter 7 in the SI). While **G1** did not show a strong binding to cage **1**, chemical shift perturbations of the NMR signals of cage **2** point towards strong interactions between cage **2** and **G1** (see Fig. S62–S65 in the SI). While protons a^2 and d^2 of the Zn_2L unit are downfield shifted, the upfield shift of the protons b^2 and c^2 of the triazine unit point towards shielding. These shift changes are in accordance with the effect of the ring current of **G1**. The significant broadening of the signals of **G1** in combination of the absence of additional signals indicate guest exchange on the intermediate chemical shift timescale. A job plot confirmed the expected 1 : 1 stoichiometry of cage **2** and **G1** (see Fig. S66 and S67 in the SI). This finding aligns perfectly with the cavity size measures, as the approximately 7 Å distance between the tritopic triazine ligands **B** provides an ideal spacing for π–π stacking with **G1**. A binding constant of K_a = 1.77 × 10^3 M^{-1} was determined by ^{1}H NMR titration studies (see Fig. S68 and S69 in the SI). The strongly differentiated binding behaviour can be attributed to the smaller cavity of cage **2** compared to cage **1**. Furthermore, the twisting of the phenyl units of **A** within cage **1** might prevent strong attractive π–π interactions of **G1** with cage **1**.

In contrast to the weak interactions of cage **1** and **G1**, strong interactions between cage **1** and **G2** were observed (see Fig. S70 and S71 in the SI). These result in downfield shifts of protons a^1, c^1, e^1 and i^1 and upfield shifts of protons b^1, d^1, f^1, and h^1. In particular, the protons of ligand **A** exhibit pronounced shielding, evidenced by substantial upfield shifts of up to 0.6 ppm which can be explained by **G2**'s ring current effect. The addition of up to 1 eq. of **G2** results in a significant broadening of the signals, which are sharpening after addition of further **G2**. The addition of more than 5 eq. of **G2** does not result in further signal sharpening and shifting anymore,

pointing towards a rather strong binding of **G2** by cage **1**. The determination of a binding stoichiometry and constant was not possible due to partial decomposition of the cages after addition of more than 1 eq. of **G2**. For that reason, possible emission quenching effects were not investigated. Besides quantitative differences, the guest binding of **G2** to cage **2** results in similar chemical shift perturbations as observed for cage **1**. Downfield shifts were observed for the $\mathbf{Zn_2L}$ protons a^2, e^2, d^2 and h^2, while strong upfield shifts were obtained for the protons b^2 and c^2 of the triazine ligand **B** (see Fig. S72 and S73 in the SI). Guest encapsulation of **G2** results also in a partial decomposition of the cage, preventing binding constant determination. However, the significant shift changes upon addition of **G2** in combination with the absence of further shifts after addition of 1 eq. **G2** suggests a 1 : 1 binding stoichiometry. The stronger binding of **G2** with cage **2** compared to cage **1** might be based on the different cavity measures of cage **2** in combination with stronger π–π stacking with the planar tritopic **B** ligand.

Conclusions

Here we establish the Zn(II) bis-salphen unit $\mathbf{Zn_2L}$ as a novel building unit for heteroleptic coordination cages. Upon self-assembly with tritopic ligands, trigonal prismatic cages were obtained in a quantitative manner. While dilution experiments confirmed the high stability of these cages even at low concentrations, a highly dynamic nature was observed at high concentrations allowing the formation of a mixed cage. The nature of the tritopic ligand **A** and **B** strongly alters the optical properties, as we observed an orange emission with a quantum yield of $\Phi_{\mathbf{1,DCM}}$ = 6.6% for cage **1**, while cage **2** is non-emissive. The emission is based on the $\mathbf{Zn_2L}$ building unit and the emission quenching of cage **2** can be attributed to the electron withdrawing effect of the triazine containing ligand **B**. To investigate the guest binding potential of the two novel structures, host–guest studies were performed with the phenyl-derivates of the tritopic ligands. While both cages showed binding towards the triazine-based guest **G2**, addition of **G2** in excess results in a partial decomposition of the cages. As we assume that this decomposition will be even stronger at low concentrations that are required for optical studies, the optical sensor behaviour could not be investigated in detail. However, our results prove that the Zn(II) bis-salphen unit $\mathbf{Zn_2L}$ qualifies as a highly promising building unit for emissive heteroleptic coordination cages. To unlock the full application potential of the bis-salphen based cages, follow-up studies will focus on the increase of their robustness to further pave the way for their usage as optical sensors.

Author contributions

L. D. wrote the first draft of the manuscript and performed the synthesis and characterization of the cages. K. S. performed the DOSY measurements of the cages. F. W. H. performed the single-crystal structure analysis of cage **1** and **2**. J. H. supervised DOSY experiments and edited the manuscript. H. K. performed the optical measurements, corrected the manuscript and led the project. All co-authors contributed to the correction of the final manuscript.

Conflicts of interest

There are no conflicts to declare.

Data availability

The data supporting this article have been included as part of the supplementary information (SI). Supplementary information is available. See DOI: https://doi.org/10.1039/d5nr04564a.

CCDC 2497733 (**1**) and 2497723 (**2**) contain the supplementary crystallographic data for this paper and can be obtained free of charge from www.ccdc.cam.ac.uk/structures.[49a,b]

Acknowledgements

We thank the North Bavarian NMR Centre (NBNC) and the Central Analytics of the Department of Chemistry of the University of Bayreuth for analytical measurements. We thank Prof. Dr Henry Dube, Dr Frank Hampel, and Bernadeta Hack from the University of Erlangen-Nuremberg for high-resolution ESI-TOF MS measurements.

References

1 P. Mal, B. Breiner, K. Rissanen and J. R. Nitschke, *Science*, 2009, **324**, 1697–1699.
2 D. Fujita, R. Suzuki, Y. Fujii, M. Yamada, T. Nakama, A. Matsugami, F. Hayashi, J.-K. Weng, M. Yagi-Utsumi and M. Fujita, *Chem*, 2021, **7**, 2672–2683.
3 J. A. Robson and I. A. Riddell, in *Reactivity in Confined Spaces*, ed. G. Lloyd and R. S. Forgan, The Royal Society of Chemistry, 2021, pp. 108–132.
4 T. K. Piskorz, V. Martí-Centelles, R. L. Spicer, F. Duarte and P. J. Lusby, *Chem. Sci.*, 2023, **14**, 11300–11331.
5 M. D. Ward, *Chem. Commun.*, 2024, **60**, 10464–10475.
6 D. Liu, H. Ma, C. Zhu, F. Qiu, W. Yu, L.-L. Ma, X.-W. Wei, Y.-F. Han and G. Yuan, *J. Am. Chem. Soc.*, 2024, **146**, 2275–2285.
7 D. Zhang, T. K. Ronson, Y.-Q. Zou and J. R. Nitschke, *Nat. Rev. Chem.*, 2021, **5**, 168–182.
8 W.-Y. Zhang, Y.-J. Lin, Y.-F. Han and G.-X. Jin, *J. Am. Chem. Soc.*, 2016, **138**, 10700–10707.
9 X. Zhang, D. Zhang, C. Wei, D. Wang, R. Lavendomme, S. Qi, Y. Zhu, J. Zhang, Y. Zhang, J. Wang, L. Xu, E.-Q. Gao, W. Yu, H.-B. Yang and M. He, *Nat. Commun.*, 2024, **15**, 3766.

10 M. Yamashina, M. M. Sartin, Y. Sei, M. Akita, S. Takeuchi, T. Tahara and M. Yoshizawa, *J. Am. Chem. Soc.*, 2015, **137**, 9266–9269.
11 Z. Zhang, Z. Zhao, L. Wu, S. Lu, S. Ling, G. Li, L. Xu, L. Ma, Y. Hou, X. Wang, X. Li, G. He, K. Wang, B. Zou and M. Zhang, *J. Am. Chem. Soc.*, 2020, **142**, 2592–2600.
12 J. S. Train, A. B. Wragg, A. J. Auty, A. J. Metherell, D. Chekulaev, C. G. P. Taylor, S. P. Argent, J. A. Weinstein and M. D. Ward, *Inorg. Chem.*, 2019, **58**, 2386–2396.
13 C. J. T. Cox, J. Hale, P. Molinska and J. E. M. Lewis, *Chem. Soc. Rev.*, 2024, **53**, 10380–10408.
14 H. Kurz, P. C. P. Teeuwen, T. K. Ronson, J. B. Hoffman, P. Pracht, D. J. Wales and J. R. Nitschke, *J. Am. Chem. Soc.*, 2024, **146**, 30958–30965.
15 A. J. McConnell, *Chem. Soc. Rev.*, 2022, **51**, 2957–2971.
16 B. S. Pilgrim and N. R. Champness, *ChemPlusChem*, 2020, **85**, 1842–1856.
17 A. Platzek, S. Juber, C. Yurtseven, S. Hasegawa, L. Schneider, C. Drechsler, K. E. Ebbert, R. Rudolf, Q. Yan, J. J. Holstein, L. V. Schäfer and G. H. Clever, *Angew. Chem., Int. Ed.*, 2022, **61**, e202209305.
18 W. M. Bloch, J. J. Holstein, W. Hiller and G. H. Clever, *Angew. Chem., Int. Ed.*, 2017, **56**, 8285–8289.
19 E. Benchimol, I. Regeni, B. Zhang, M. Kabiri, J. J. Holstein and G. H. Clever, *J. Am. Chem. Soc.*, 2024, **146**, 6905–6911.
20 M. Yoshizawa, M. Nagao, K. Kumazawa and M. Fujita, *J. Organomet. Chem.*, 2005, **690**, 5383–5388.
21 D. Preston, J. E. Barnsley, K. C. Gordon and J. D. Crowley, *J. Am. Chem. Soc.*, 2016, **138**, 10578–10585.
22 Y. Yamauchi, M. Yoshizawa, M. Akita and M. Fujita, *J. Am. Chem. Soc.*, 2010, **132**, 960–966.
23 M. L. Saha, S. Neogi and M. Schmittel, *Dalton Trans.*, 2014, **43**, 3815–3834.
24 Y.-R. Zheng, Z. Zhao, M. Wang, K. Ghosh, J. B. Pollock, T. R. Cook and P. J. Stang, *J. Am. Chem. Soc.*, 2010, **132**, 16873–16882.
25 C. García-Simón, M. Garcia-Borràs, L. Gómez, I. Garcia-Bosch, S. Osuna, M. Swart, J. M. Luis, C. Rovira, M. Almeida, I. Imaz, D. Maspoch, M. Costas and X. Ribas, *Chem. – Eur. J.*, 2013, **19**, 1445–1456.
26 M. Zhang, M. L. Saha and P. J. Stang, *Struct. Chem.*, 2017, **28**, 453–459.
27 W. M. Bloch, Y. Abe, J. J. Holstein, C. M. Wandtke, B. Dittrich and G. H. Clever, *J. Am. Chem. Soc.*, 2016, **138**, 13750–13755.
28 S. Mukherjee and P. S. Mukherjee, *Chem. Commun.*, 2014, **50**, 2239–2248.
29 Y. Hou, Z. Zhang and M. Zhang, *Acc. Chem. Res.*, 2025, **58**, 1644–1656.
30 T. Abe, N. Sanada, K. Takeuchi, A. Okazawa and S. Hiraoka, *J. Am. Chem. Soc.*, 2023, **145**, 28061–28074.
31 L. A. V. Faulkner and J. D. Crowley, *Chem*, 2024, **10**, 440–442.
32 K. Wu, E. Benchimol, A. Baksi and G. H. Clever, *Nat. Chem.*, 2024, **16**, 584–591.
33 L. L. K. Taylor, R. Andrews, A. C. Y. Sung, I. J. Vitorica-Yrezabal and I. A. Riddell, *Chem. Commun.*, 2022, **58**, 12301–12304.
34 J. A. Davies, T. K. Ronson and J. R. Nitschke, *J. Am. Chem. Soc.*, 2024, **146**, 5215–5223.
35 Y. Du, T. K. Ronson, Y. Yang and J. R. Nitschke, *J. Am. Chem. Soc.*, 2025, **147**, 43927–43933.
36 Y.-X. Chen, H.-L. Yue, Y.-Q. Wu, M. Yu and J. Tao, *J. Am. Chem. Soc.*, 2025, **147**, 47311–47321.
37 B. Zhang, H. Lee, J. J. Holstein and G. H. Clever, *Angew. Chem., Int. Ed.*, 2024, **63**, e202404682.
38 A. W. Kleij, M. Kuil, D. M. Tooke, M. Lutz, A. L. Spek and J. N. H. Reek, *Chem. – Eur. J.*, 2005, **11**, 4743–4750.
39 M. Kuil, P. E. Goudriaan, A. W. Kleij, D. M. Tooke, A. L. Spek, P. W. N. M. Van Leeuwen and J. N. H. Reek, *Dalton Trans.*, 2007, 2311.
40 J. Zhao, F. Dang, B. Liu, Y. Wu, X. Yang, G. Zhou, Z. Wu and W.-Y. Wong, *Dalton Trans.*, 2017, **46**, 6098–6110.
41 S. J. Wezenberg, E. C. Escudero-Adán, J. Benet-Buchholz and A. W. Kleij, *Inorg. Chem.*, 2008, **47**, 2925–2927.
42 M. M. Belmonte, S. J. Wezenberg, R. M. Haak, D. Anselmo, E. C. Escudero-Adán, J. Benet-Buchholz and A. W. Kleij, *Dalton Trans.*, 2010, **39**, 4541.
43 G. Consiglio, S. Failla, P. Finocchiaro, I. P. Oliveri, R. Purrello and S. Di Bella, *Inorg. Chem.*, 2010, **49**, 5134–5142.
44 G. Consiglio, S. Failla, P. Finocchiaro, I. P. Oliveri and S. D. Bella, *Dalton Trans.*, 2012, **41**, 387–395.
45 H. Kurz, G. Hörner, O. Weser, G. Li Manni and B. Weber, *Chem. – Eur. J.*, 2021, **27**, 15159–15171.
46 J. B. Maglic and R. Lavendomme, *J. Appl. Crystallogr.*, 2022, **55**, 1033–1044.
47 G. Montà-González, F. Sancenón, R. Martínez-Máñez and V. Martí-Centelles, *Chem. Rev.*, 2022, **122**, 13636–13708.
48 S. Mecozzi and J. Rebek Jr., *Chem. – Eur. J.*, 1998, **4**, 1016–1022.
49 (*a*) CCDC 2497733: Experimental Crystal Structure Determination, 2026, DOI: 10.5517/ccdc.csd.cc2pv31q; (*b*) CCDC 2497723: Experimental Crystal Structure Determination, 2026, DOI: 10.5517/ccdc.csd.cc2pv2qc.